Available online at www.sciencedirect.com
SCIENCE DIRECT®
Journal of Inorganic Biochemistry 99 (2005) 1973–1982
Journal of Inorganic Biochemistry
www.elsevier.com/locate/jinorgbio

Heterometallic manganese/zinc-phytate complex as a model compound for metal storage in wheat grains

Ubirajara P. Rodrigues-Filho [a,*], Silvio Vaz Jr. [a], Marcella P. Felicissimo [a], Marciela Scarpellini [a,1], Daniel R. Cardoso [a], Rita C.J. Vinhas [b], Richard Landers [b], Jose F. Schneider [c], Bruce R. McGarvey [d], Mogens L. Andersen [e], Leif H. Skibsted [e]

[a] *Instituto de Química de São Carlos, Universidade de São Paulo, 13564-970, São Carlos, Brazil*
[b] *Instituto de Física Gleb Wataguin, Universidade Estadual de Campinas, Campinas, Brazil*
[c] *Instituto de Física de São Carlos, Universidade de São Paulo, 13564-970, São Carlos, Brazil*
[d] *Department of Chemistry and Biochemistry, Windsor University, Windsor, Ont., Canada, N9B 3P4*
[e] *Department of Food Chemistry, The Royal Veterinary and Agricultural University (KVL), Frederiksberg, Denmark*

Received 31 March 2005; received in revised form 10 June 2005; accepted 13 June 2005
Available online 27 July 2005

Abstract

Myo-inositol-1,2,3,4,5,6-hexakisphosphate, also known as phytate, is a natural metal chelate present in cereals, an important feedstock worldwide. This article reports the characterization of three metal storage model complexes: the homometallic Mn(II) myo-inositol-1,2,3,4,5,6-hexakisphosphate (IP6), the heterometallic Zn(II), Mn(II) analogue $Na_4MnZn_4(C_6H_6O_{24}P_6)\cdot(NO_3)_2\cdot 8H_2O$ ($MnZn_4IP6$) and the homometallic Zn(II) metal complex $Na_3Zn_5(C_6H_6O_{24}P_6)OH\cdot 9H_2O$ (Zn_5IP6). The techniques of high-resolution ^{23}Na, ^{13}C and ^{31}P NMR, electron paramagnetic resonance (EPR) and X-ray photoelectron spectroscopy (XPS) were applied in this study. The complexation of Zn(II) and Mn(II) by phosphate groups of IP6 is demonstrated by NMR and XPS results. ^{13}C NMR results show a conformation for IP6 consisting of five equatorial phosphate groups to one axial group showing only one chemical environment for Zn and two for Mn, when characterized by XPS and EPR, in both Mn complexes. These results support, for the first time, a probable supramacromolecular structure for phytate complexes of transition metals. Based on the similarity between the EPR spectra of wheat seeds and that of the $MnZn_4IP6$ compound, the manganese storage centers in wheat grains can be assigned to similar heterometallic phytate complexes.

Keywords: Wheat; Manganese storage compounds; Zn(II) storage compounds; Myo-inositol-1,2,3,4,5,6-hexakisphosphate; Phytate; EPR; XPS; MAS NMR; Metal storage in plants; Manganese bioavailability

1. Introduction

The myo-inositol-1,2,3,4,5,6-hexakisphosphate (IP6), phytate, is the major phosphorous component of plants and special cereal grains [1,2]. Phytate has long been known as an antinutritional factor since it binds nutrient mineral cations, especially from milk products, making them unavailable for nourishing the body and therefore interfering in their homeostasis [3–6]. Phytate is present in several foods and especially large values have been

* Corresponding author. Present address: Laboratoire de Physique de la Matière Condensée, École Polytechnique, 91128 Palaiseau Cedex, France. Tel.: +33 1 69 33 39 97; fax: +33 1 69 33 30 04.
E-mail addresses: bira.rodrigues@polytechnique.fr, br@pmc.polytechnique.fr (U.P. Rodrigues-Filho).
[1] Present address: University of Michigan, Department of Chemistry, Willard H. Dow Laboratories, 930 North University, Ann Arbor, MI 48108, USA.

0162-0134/$ - see front matter © 2005 Elsevier Inc. All rights reserved.
doi:10.1016/j.jinorgbio.2005.06.014

found in roasted peanuts, dry roasted cashews, shredded wheat cereals and wheat flour [7]. Therefore, phytate is of concern in diets based on cereals and nuts. Interest in these inositol phosphate compounds has increased since it has been proposed that they have roles as an antioxidant [8], as a secondary messenger and DNA repair agent [9] and for treatment of calcium oxalate renal lithiaisis [10].

In plants, phytic acid is responsible for 50–80% of the total phosphorous content [11] and therefore plays an important role in phosphorus storage. In cereal seeds, phytic acid is mainly located in globoid agglomerates in the aleuronic layer region [11]. The interest in studying the interaction of the manganese ion with phytate is due to the important micronutrient role of this metal for plants, and to the fact that phytate can play a role for manganese homeostasis in plants. Few authors have reported data on the molecular structure of transition metal phytate complexes. Gerard et al. [12] reported a tetrahedral structure for soluble Zn(II) phytate and cobalt phytate complexes based on potentiometric studies, ^{31}P NMR and UV–visible spectroscopy. Pierce [13] reported enthalpic results obtained from Differential Scanning Calorimetric and thermogravimetric analysis of non-crystalline insoluble complexes of polynuclear Zn(II) phytate with water coordinated to the metal centers. The isolated Zn(II) phytate had a Zn(II):IP6 ratio of 5:1.

In this paper, we report the synthesis and characterization of the insoluble Zn(II) and Mn(II) complexes of phytate as model complexes for manganese storage in wheat seeds. To investigate the chemical structure of the $MnZn_4IP6$, Mn_5IP6 and Zn_5IP6 model compounds, the following techniques were applied: elemental analysis, infrared absorption spectroscopy (FT-IR), multinuclear magnetic resonance spectroscopy with magic angle spinning (MAS NMR), X-ray photoelectron spectroscopy (XPS), and electron paramagnetic resonance (EPR). In addition, EPR analyses of wheat seeds and flour from different parts of the world (Brazil and Denmark) are reported to help identify possible manganese storage compounds in cereals.

2. Experimental

2.1. Materials

Dodecasodium phytate, IP6, was used as supplied from Sigma (St. Louis, USA). Manganese perchlorate was supplied from Aldrich (St. Louis, USA), triethylamine was supplied by Acros (Geel, Belgium), and Zn(II) nitrate was supplied by Vetec (São Paulo, Brazil). The water used for the synthesis was de-ionized water with a resistivity of 18 MΩ. Methanol was supplied by Vetec (São Paulo, Brazil).

The Brazilian wheat seed was kindly supplied by EMBRAPA Trigo, Rio Grande do Sul. The Danish wheat seed were winter variety (Bunker for biscuits) kindly supplied by the Department of Food Science, Cereal Group of The Royal Veterinary and Agricultural University (KVL), Frederiksberg, Denmark. The wheat flour obtained from a special wheat varietal for biscuits was provided by Biska (Hiørring, Denmark).

2.2. Syntheses

2.2.1. Manganese phytate synthesis, $(Na_3Mn_5(C_6H_6O_{24}P_6)OH \cdot 9H_2O)$, Mn_5IP6

Two hundred fifty milligrams (0.25 g) of dodecasodium phytate (0.27 mmol) were diluted in 21 mL of a methanol:de-ionized water mixture (20:1, v:v). Then, 0.20 mL of triethylamine and 10.0 mL of methanol solution of $Mn(ClO_4)_2 \cdot 6H_2O$ (0.27 g, 0.75 mmol) were added, under stirring and heating at ~60 °C for 3 h. The solution pH during the synthesis was between 7 and 8. A dark brown precipitate was collected by vacuum filtration. The yield of $Na_3Mn_5(C_6H_6O_{24}P_6)OH \cdot 9H_2O$ was 63% based on manganese perchlorate.

2.2.2. Zinc phytate synthesis, $Na_3Zn_5(C_6H_6O_{24}P_6)OH \cdot 9H_2O$, Zn_5IP6

Two hundred fifty milligrams (0.25 g) of dodecasodium phytate (0.27 mmol) was diluted in 40 mL of methanol:de-ionized water (1:1, v:v). Afterwards, 0.20 mL of triethylamine and 0.27 g of $Zn(NO_3)_2 \cdot 6H_2O$ (1.2 mmol) were added, under continuous stirring and heating at ~60 °C for 3 h. The solution pH during the synthesis was between 7 and 8. A white powder was precipitated and was collected by vacuum filtration. The yield of $Na_3Zn_5(C_6H_6O_{24}P_6)OH \cdot 9H_2O$ was 70% based on zinc nitrate.

2.2.3. Heterometallic zinc/manganese phytate synthesis, $Na_4MnZn_4(C_6H_6O_{24}P_6) \cdot (NO_3)_2 \cdot 8H_2O$, $MnZn_4IP6$

The heterometallic compound was prepared in a similar procedure to that used for the $Na_3Zn_5(C_6H_6O_{24}P_6)OH \cdot 9H_2O$ by mixing 0.27 g of $Zn(NO_3)_2 \cdot 6H_2O$ (1.2 mmol) and 0.0018 g (5.0 μmol) of $Mn(ClO_4)_2 \cdot 6H_2O$. The solution pH during the synthesis was between 7 and 8. The $Na_4MnZn_4(C_6H_6O_{24}P_6) \cdot (NO_3)_2 \cdot 8H_2O$ yield was 70% based on manganese perchlorate.

Each synthesis has been repeated and the data reported herein are the average of several measurements.

2.3. Elemental analysis

All samples were dried under vacuum, ≈626 mmHg, at 353 K for 2 h in a MA 030, MARCONI oven (Piracicaba, Brazil). They were analyzed in an EA1110 CHNS-O, CE INSTRUMENTS elemental analyzer equipment (Milan, Italy).

2.4. Magic angle spinning nuclear magnetic resonance

High-resolution solid-state ^{13}C NMR measurements were carried out in a Varian Unity INOVA spectrometer at a field of 9.4 T, using a 7 mm magic angle spinning (MAS) probe. Samples were spun up to 7 kHz in silicon nitride rotors. Spectra were measured with a single pulse excitation and also by ^{1}H–^{13}C cross-polarization (CP) technique. The CP experiment was carried out using a $\pi/2$ ^{1}H pulse of 3.5 μs, contact time of 1 ms, recycle delay of 30 s and ^{1}H decoupling of 80 kHz. In single pulse experiments a $\pi/2$ pulse of 3.5 μs was used with recycle delay of 30 s and ^{1}H decoupling of 80 kHz. Also, the delayed ^{1}H decoupling technique was used to suppress non-quaternary carbon signals, using a delay time of 30 μs between the end of the excitation pulse and the beginning of the decoupling irradiation [14]. ^{31}P NMR experiments were carried out using a $\pi/2$ pulse of 4.0 μs, recycle delay of 400 s and ^{1}H decoupling. ^{23}Na NMR experiments were carried out using a $\pi/16$ pulse of 0.5 μs, recycle delay of 2 s, and no ^{1}H decoupling. References for chemical shift of ^{13}C, ^{31}P and ^{23}Na were TMS, 85% H_3PO_4 and 0.1 M NaCl, respectively.

2.5. X-ray photoelectron spectroscopy

The XPS measurements were performed in an OHMNICROM spectrometer using non-monochromatic Al Kα radiation (1486.6 eV, power of 140 W) and a hemispherical analyzer with pass energy of 44 eV. The base pressure in the chamber was in the range of 10^{-9} Torr. The spectra were charge-corrected using the Na1s binding energy at 1071.3 eV for Na_3PO_4 [15] as well as the C1s at 286.6 eV for myo-inositol [16]. The atomic ratios were calculated using the Scofield cross-sections [17].

All XPS peaks of insulating samples were fitted according to the Leclercq and Pireaux's method, using Gaussian–Lorentzian peaks [18].

2.6. Infrared absorption spectroscopy

The infrared absorption spectra of the samples were acquired in the transmission mode using KBr pellets of the samples at weight-to-weight ratio of 1:100. The samples were previously dried under vacuum at 353 K for 1 h. The spectra were obtained in a BOMEM MB-102 spectrophotometer (Quebec, Canada).

2.7. Electron paramagnetic resonance

The solid-state EPR spectra were recorded using previously dried samples in a quartz tube in an X-band CW ESP 300E Bruker (Karlsruhe, Germany) spectrometer. The modulation amplitude was 5.1 G for the wheat grains or 0.4 G for the model compounds, modulation frequency of 100 kHz. All spectra were run at room temperature unless otherwise noted.

3. Results

3.1. Electron paramagnetic resonance spectroscopy

Six-line Mn(II) EPR signals have not only been observed in wheat kernels [19], but also in several plant derived foods such as coconut milk [20], apples [21], green tea [22,23], raspberry [24], and coffee [25]. Similar spectra have also been observed in several types of human tissues and bodily fluids [26].

The spectra of flours from Biska (Denmark) and wheat seeds from Denmark and Brazil showed the same features, a weak free radical signal at $g = 2.00$, $\Delta H_{pp} = 6$ G, probably due to nitrogen-centered radicals in the gluten formed by peptide scission [27] and a more intense broad line centered around $g = 2$ with a sextet signal attributed to Mn(II) (Fig. 1(a) and (c)). This sextet signal is typical of Mn(II) ions, which have a sextet hyperfine splitting due to the $I = 5/2$ nuclear spin of the ^{55}Mn nucleus. The husks of the seeds showed a higher intensity for the sextet lines than for the embryo part. Based on the literature [11], we supposed the Mn(II) compound to be a manganese-phytate complex and therefore a model complex was prepared in vitro. This manganese-phytate complex (Mn_5IP6) showed an EPR spectrum with an inhomogeneous line broadened by magnetic dipole–dipole interactions between the Mn(II) centers, $\Delta H_{pp} = (644 \pm 80)$ G (Figure S1). We decided to synthesize a heterometallic Zn/Mn species ($MnZn_4$-IP6) as phytate has been claimed to be associated

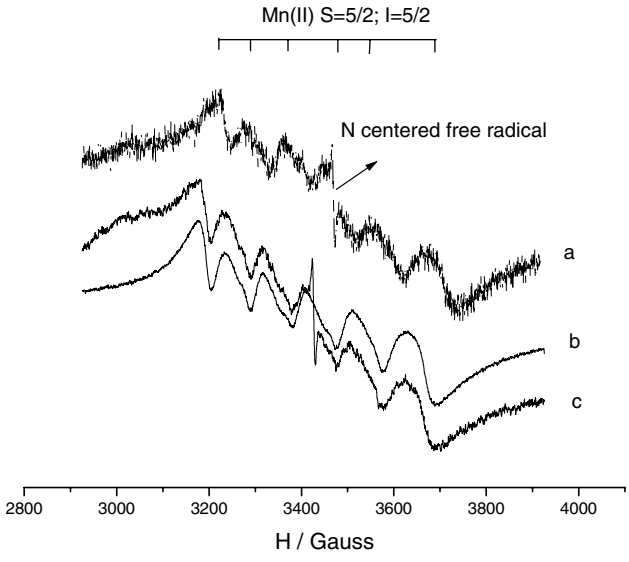

Fig. 1. EPR spectra of (a) Brazilian wheat seed and (b) model $MnZn_4IP6$ compound and (c) Danish wheat seed.

with Zn(II), calcium and manganese in cereals [11] and also because the Zn(II) would magnetically dilute the manganese, preventing dipolar interactions thus reducing the line broadening. The spectrum obtained from the heterometallic species, $MnZn_4IP6$, (Fig. 1(b)), displays a Mn(II) hyperfine line pattern very similar to the signal observed for the wheat seeds and flours except for the absence of the free radical signal.

The spectrum of $MnZn_4IP6$ is similar to that of the two flours except for the absence of a free radical signal. The sextet portion of the three spectra is very similar but the intensity of the broad line relative to the sextet appears to be larger in the flour samples. Unless the zero field interaction is very small, the observed sextet feature is due to the central fine structure line, $M_S = -1/2$ to 1/2 transition. The four other fine structure lines constitute part or all of the broader line.

The Mn(II) is an ^6S ion with $S = 5/2$ whose EPR spectra is normally fitted to the spin Hamiltonian

$$H = \beta_e[g_x S_x H_x + g_y S_y H_y + g_z S_z H_z] + D\left[S_z^2 - \frac{35}{12}\right] + E[S_x^2 - S_y^2] + [A_{xx} S_x I_x + A_{yy} S_y I_y + A_{zz} S_z I_z], \quad (1)$$

where H is the magnetic field, S is the electron spin operator, I is the nuclear spin operator, and β_e is the Bohr magneton. The g_i, A_{ii}, D and E parameters are spin Hamiltonian parameters to be determined experimentally. For Mn(II), an ^6S state ion, A and g parameters are generally isotropic with values of 85–95 G and 2.00, respectively. By definition, the magnitude of the zero field parameter E can be no larger that one-third that of the D parameter and $D = 0$ for octahedral or tetrahedral sites. In powder spectra of systems with D greater in magnitude than the spectrometer's photon, which in our case is 0.3 cm^{-1}, a prominent peak appears around $g = 4.3$ when $|E| \approx |D|/3$ and several peaks appear if E is smaller in magnitude. The absence of lines in $g = 4.3$ region is indicative of the magnitude of D being less than 0.3 cm^{-1} [28,29].

We have used a simulation program obtained from Dr. Hogni Weihe (Department of Chemistry, University of Copenhagen, Universitetsparken 5, DK 2100 Copenhagen, Denmark, weihe@kiku.dk), which can produce simulations using the spin Hamiltonian given in Eq. (1) with a personal computer in a DOS environment, to simulate the spectrum of $MnZn_4IP6$. Indeed, if we assumed only one species of Mn(II), it was not possible to simulate the spectrum (Figure S2). The narrow sextet which is unevenly spaced and the presence of more than one line in the second, third and fourth hyperfine lines, counting from the left, in the spectrum could be reasonably simulated using the parameters of $D = 0.014$ cm^{-1}, $E = 0.00467$ cm^{-1}, $A = 95$ G, $g = 2.003$, with a line-width parameter of 42 G and a Lorentzian line shape. The line-width parameter is the width of the absorption line at half height. The success of this simulation showed us that the odd splitting pattern and the presence of more than six lines was not due to two separate species but rather to the presence of electron spin–nuclear spin double flips and the consequent distortion of intensities in the "allowed transitions". This simulation did not, however, explain the broad tails and the extra width of the outside pair of hyperfine lines. Further, it produced narrow peaks for the Fine structure lines due to $M_S = \pm 1/2 \leftrightarrow \pm 3/2$ and $\pm 3/2 \leftrightarrow \pm 5/2$ transitions. We presumed these peaks are further broadened due to different Mn(II) sites on the IP6 ring with different values of D and E. Since the center sextet is affected by the second-order term in D and E while the other fine structure lines are affected by a first-order term, a 10% change in D will only produce a 1% change in the center sextet. We evaluated this effect by simulating three lines with $D = 0.015$, 0.014 and 0.013 cm^{-1} with $E = D/3$ and then averaged the three spectra (Figure S2A). This effectively broadened the peaks in the tail without affecting the center sextet but did not improve the simulation of the tails which really required a larger D value and larger line-width parameter. Therefore, we simulated a spectrum for $D = 0.02$ cm^{-1} and $E = 0.00667$ cm^{-1} with the same g and A values but with a line-width parameter of 200 G (Figure S2B). In order to estimate the relative concentration of these Mn species in the $MnZn_4IP6$ complex we used the area under the EPR absorption. The ratio between the two types of Mn from EPR experimental spectrum was 1:2. Then, we combined the two simulations in the ratio of one part of the averaged narrow line to 2 parts of the broad line to get the simulation shown in Fig. 2. The simulation seems good enough to conclude the spectrum is due to two main types of Mn(II).

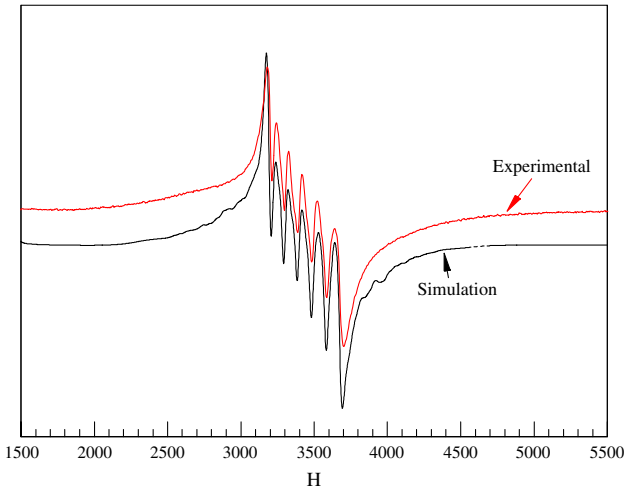

Fig. 2. Comparison of simulated EPR signal using parameters described in the text to that of the experimental spectrum for $MnZn_4IP$.

Table 1
Elemental analysis results for %C, %H, %N and Mn/Na and Mn/P atomic ratios obtained by XPS

Sample	Organic elemental analysis			XPS atomic ratios	
	%C	%H	%N	Mn/P	Mn/Na
Mn/IP6	6.7	2.2	0	0.86	1.67
Zn(II)/IP6	5.8	2.6	0	0.80	

3.2. Elemental analysis

The C, H and N content determined by elemental analysis of the Mn_5IP6, and XPS atomic ratio from the XPS high-resolution results, Table 1, suggest that the $Na_3Mn_5(C_6H_6O_{24}P_6)OH \cdot 9H_2O$ molecular formula. The results for the Zn_5IP6 and $MnZn_4IP6$ suggest that the molecular formulas $Na_3Zn_5(C_6H_6O_{24}P_6)OH \cdot 9H_2O$ and $Na_4MnZn_4(C_6H_6O_{24}P_6) \cdot (NO_3)_2 \cdot 8H_2O$, respectively.

3.3. Infrared absorption spectroscopy

The FT-IR spectra of the Mn_5IP6, Zn_5IP6 and $MnZn_4IP6$ showed the δ_{O-P-O}, $\nu_{P=O}$, ν_{P-O} and ν_{P-O-C} peaks in the same region at (541.5 ± 2.0), (1392.0 ± 4.0), (848.0 ± 4.0), (993.5 ± 4.0) and $(1124.0 \pm 3.0)\ cm^{-1}$, respectively (Figure S3). The $\nu_{P=O}$ and ν_{P-O} are closer than observed in the dodecasodium phytate and the δ_{O-P-O} is shifted toward lower wave number showing the transition metals are coordinated to the phosphate group of phytic acid, $R–OPO_3^{2-}$. The decrease in the separation between the $\nu_{P=O}$ and ν_{P-O} is symptomatic of a probable bidentate coordination [30].

3.4. Solid-state NMR

Fig. 3(a) shows the ^{13}C NMR spectrum of IP6, composed of two partially resolved lines at 74 and 67 ppm with a respective intensity ratio of 5:1. These values are compatible with the chemical shift measured for sodium aqueous solutions of IP6 at high pH [31], where the molecular conformation has 5 axial and 1 equatorial phosphate groups (5-ax/1-eq). For the Zn_5IP6 compound the ^{13}C signal has the two peaks at about 74 and 67 ppm similar to the IP6 in high pH (Fig. 3(b)). Thus, ^{13}C NMR confirms the presence of the IP6 skeleton in both compounds with a 5-ax/1-eq conformation. The line at 67 ppm can be attributed to the carbon corresponding to the axial phosphate group. On the other hand, a ^{13}C signal was not observed for $MnZn_4IP6$ compound, most probably due to the paramagnetism of Mn(II) ions.

Fig. 4 shows the ^{31}P NMR spectra of the three compounds. The ^{31}P spectrum of IP6 has one symmetric peak at 7.2 ppm with line-width of 5 ppm. According to the solution NMR results, the separation between

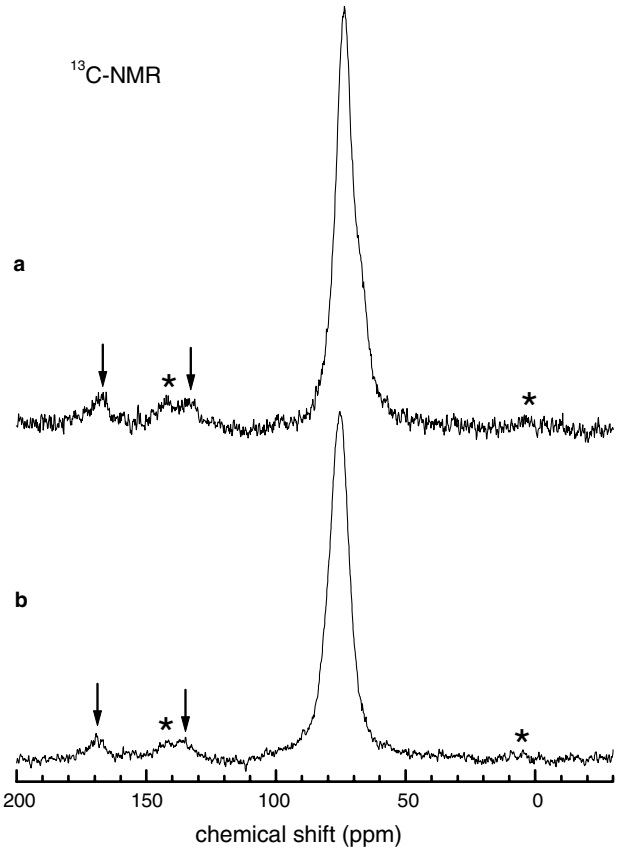

Fig. 3. ^{13}C MAS NMR spectra of IP6 (a) and ZnIP6 (b). Asterisks: spinning side-bands. Arrows: ^{13}C background signals from rotor/probe.

the six ^{31}P resonances is less than 1 ppm, which precludes the resolution of these sites in the solid state [31]. On the other hand, the ^{31}P MAS NMR spectrum of Zn_5IP6 has three peaks at 6.1, 2.6 and −1.3 ppm with line-widths of about 1.5 ppm and respective intensity ratios of 1:3:2. These values for multiplicity and intensity ratio of the NMR lines indicate the presence of three non-equivalent P-sites per molecule. The values of chemical shift of these lines are more shielded than in IP6, which is an expected behavior when ions with stronger cationic potential are brought to the second coordination sphere of P(V) [32]. This is precisely the case for Zn(II) substituting Na. Also, this kind of substitution has consequences on the nuclear magnetic dipole–dipole interaction of P with neighboring nuclei. In the solid state, ^{23}Na can establish dipolar interaction with ^{31}P, because both species have non-zero nuclear spin. The ^{23}Na isotope is 100% abundant, has $I = 3/2$ spin and a moderate gyromagnetic ratio γ. This heteronuclear dipolar coupling between ^{31}P and ^{23}Na produces some residual broadening of the NMR lines.

On the other hand, the only isotope of Zn(II) with non-zero spin is ^{67}Zn, which is only 4% abundant and has a low γ, about a quarter of that for ^{23}Na. For these reasons, the dipolar coupling with ^{31}P is negligible.

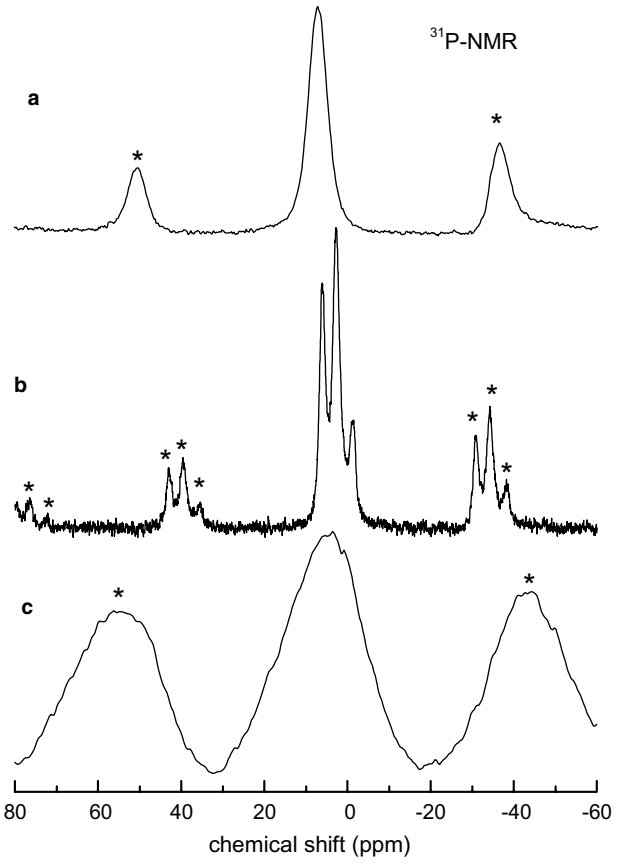

Fig. 4. ^{31}P MAS NMR spectra. (a) IP6, (b) Zn_5IP6, (c) $MnZn_4IP6$. Asterisks: spinning side-bands.

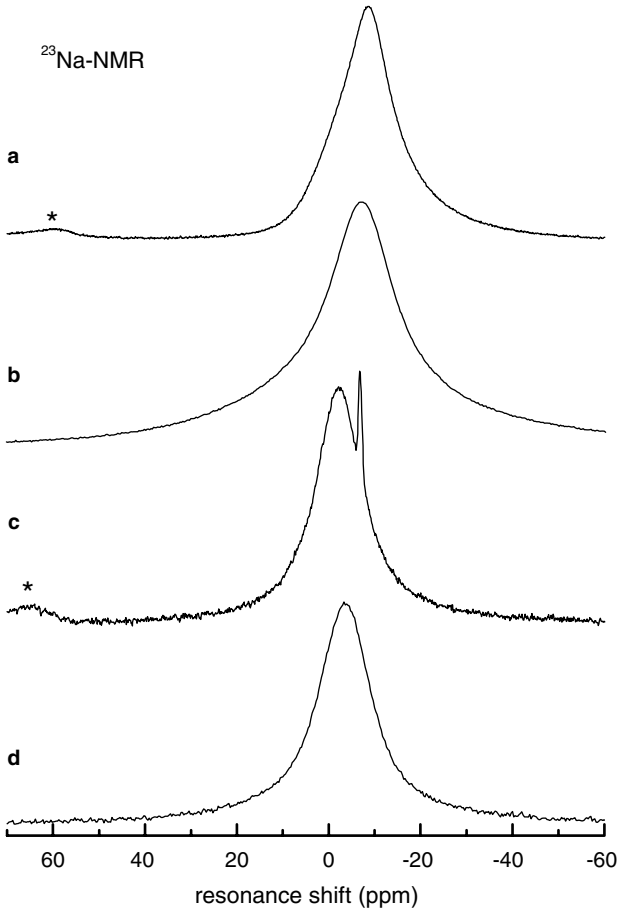

Fig. 5. MAS and static ^{23}Na NMR spectra. (a) IP6 MAS, (b) IP6 static, (c) Zn_5IP6 MAS, (d) Zn_5IP6 static.

Therefore, the substitution of Na by Zn(II) in the neighborhood of P will reduce the line-width of the NMR lines, as was observed in Fig. 4(b). Therefore, from these results we can infer the existence of a close coordination of Zn(II) ions around the IP6 molecule, causing the non-equivalence of P-sites through modifications in the molecular conformation, the shifting of the resonances due to electronic effects and the line narrowing by reducing the heteronuclear dipolar interaction. In contrast, the ^{31}P NMR spectrum of $MnZn_4IP6$ consists of a single and very broad asymmetric peak at 4 ppm with line-width of 21 ppm, resulting from paramagnetic effects (Fig. 4(c)). Not much information can be drawn from this broad line, except that Mn(II) species should be rather close to the phytate molecule.

The ^{23}Na NMR spectra of IP6 and Zn_5IP6 compounds are shown in Fig. 5. No NMR signal could be recorded for $MnZn_4IP6$, due to paramagnetic effects from Mn ions. The IP6 MAS and static spectra has a broad signal centered at −8.3 ppm with line-width of 14 ppm (Fig. 5(a) and (b)). The asymmetric line-shape may be associated to the overlapping of several site resonances and/or to the effect of second-order electric quadrupole interaction effects, which can also be dynamically modulated by diffusion-like motion of Na ions. The ^{23}Na spectrum of the Zn_5IP6 compound has two signals at −2.2 and −6.9 ppm, with respective line-widths of 12 and 0.8 ppm (Fig. 5(c)). The relative intensity of the narrower line is 3%. The extremely small line-width value, equivalent to 83 Hz, indicates the absence of second-order quadrupolar broadening. Therefore, these Na ions occupy crystal sites of cubic symmetry, which has a zero electric field gradient, or alternatively undergo fast diffusion causing motional narrowing of the quadrupolar broadening. We believe that the former hypothesis is more probable, as will be discussed later. A static NMR measurement in Zn_5IP6 (Fig. 5(d)) showed a featureless resonance with line-width of 16 ppm, very similar to the value of 12 ppm measured for the line centered at −2.2 ppm line in the MAS spectrum (Fig. 5(d)). This result indicates that Na ions contributing to the −2.2 ppm line are undergoing rapid motions, causing an efficient averaging of the anisotropic parts of the chemical shift, quadrupolar and dipolar homonuclear interactions. The MAS averaging reduces the residual anisotropy only by 25%. On the other hand, the line of minor intensity is not resolved in the static spectrum, pointing out that there exists some anisotropic broadening which is substantially

averaged out by MAS. This observation led us to propose that this narrow resonance corresponds to Na sites with low electric field gradient, giving negligible second-order quadrupolar broadening.

The anisotropic effects shown by the static experiment are associated with chemical shift interactions. Therefore, the peak position at −6.9 ppm should be attributed essentially to the isotropic chemical shift and could be assigned to Na species in cubic symmetry. These Na ions would be loosely bonded to IP6, probably in the second sphere of coordination as hydrated counter ions. The other peak would be related to Na ions more tightly bonded to phosphate groups resulting in lower symmetry and a broader line-width. Potentiometric studies in aqueous solution of phytic acid with different alkaline metals have shown a strong influence on the pK_a of this species, for instance, by formation of relatively strong complexes with phytic acid [33].

3.5. X-ray photoelectron spectroscopy

XP-spectrum of the Zn2p$_{3/2}$ region reveals for Zn_5IP6 and $MnZn_4$IP6 a symmetric peak with binding energy at 1024.2 eV. Fig. 6 shows a representative spectrum of Zn_5IP6. The symmetric peak is characteristic of only one chemical environment for Zn(II) in both complexes. The binding energy is typical of Zn(II) bound to a phosphate group [24].

The Mn2p XP-spectra of Mn_5IP6 and $MnZn_4$IP6 species show asymmetric doublets that have been fitted with two Gaussian–Lorentzian doublet functions and one singlet function, only the Mn_5IP6 spectrum is shown in Fig. 7, for illustration.

The presence of two doublets confirms the EPR hypothesis of two different chemical environments for Mn in Mn_5IP6 and $MnZn_4$IP6. Unfortunately, the Mn2p$_{3/2}$ binding energy value for these compounds,

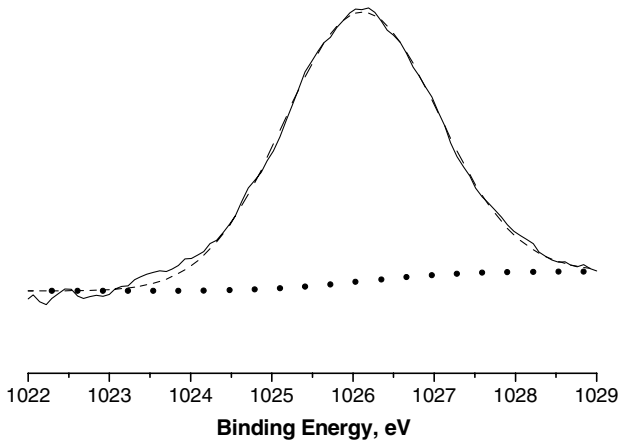

Fig. 6. XP-Zn(II)2p$_{3/2}$ spectrum of Zn_5IP6. The experimental spectrum is the straight line, fitted Gaussian–Lorentzian function is the superposed dashed line, and the dotted line is the Shirley baseline function.

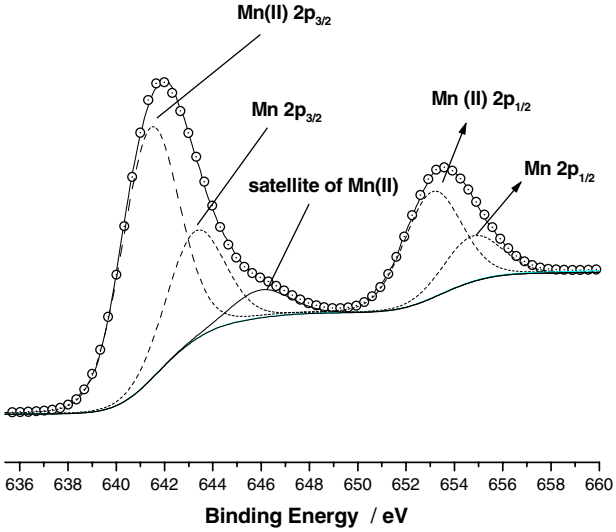

Fig. 7. Mn2p XP-spectrum of Mn_5IP6 as representative of manganese phytates. The spectrum is shown with all components used in the fitting procedure. Experimental curve is represented with dot centered circles, calculated curve is the straight line, first Mn2p doublet for Mn(II) is the dashed line in lower binding energy side, the second Mn2p doublet is the dotted line, the singlet curve in the middle of the doublets is the satellite line of the first 2p$_{3/2}$ peak.

641.4 and 643.5 eV, as well as the spin–orbit splitting in the Mn2p photoelectric peaks are not helpful in spectral assignment, since different Mn valence states have approximately the same parameters in similar chemical environments [16]. However, the presence of the shake-up satellite at 646.0 eV is an evidence of one Mn(II) species, at least, since the same is not observed for Mn(III) or Mn(IV). Petruska and Talham [35] reported Mn2p$_{3/2}$ binding energies at 643.1 eV for the manganese phosphate $Mn[O_3POC_{30}H_{47}ON_2]$, where manganese is linked to the phosphate group in a bidentate mode. Therefore, we can assign the second doublet also to a Mn(II) in a similar chemical environment as in the $Mn[O_3POC_{30}H_{47}ON_2]$. The other Mn(II) species must have a slightly different environment. Based on the lower binding energy value, 641.4 eV, observed, we assign the third doublet to a species where only one phosphate group is present and the coordination sphere is completed with water or hydroxide ions as suggested in the molecular formula. Indeed, in the Mn(OH)O compound the Mn2p$_{3/2}$ binding energy was found at 641.7 eV [16]. The coordination of water or hydroxide would result in a shift of the binding energy toward lower values as compared to species where Mn(II) is bound to two phosphate groups.

The XP-spectra of the complexes Mn_5IP6, Zn_5IP6 and $MnZn_4$IP6 in the P2p region showed an asymmetric peak that was fitted as two doublets with doublet separation for 2p$_{3/2}$ and 2p$_{1/2}$ peaks of 0.84 eV (Fig. 8). The binding energy value for the 2p$_{3/2}$ components are: (a) Mn_5IP6: 133.1 and 134.7 eV; (b) Zn_5IP6 and

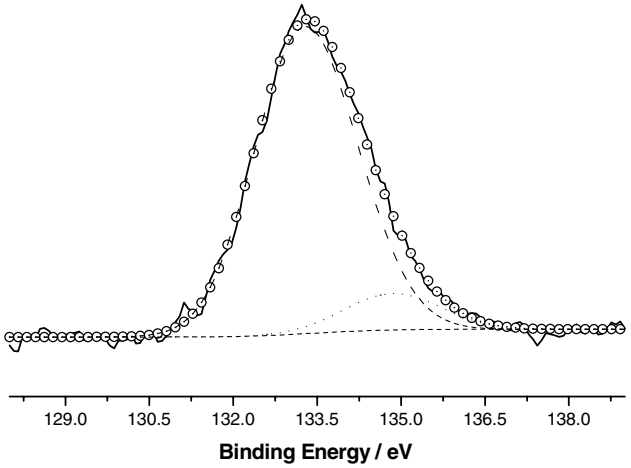

Fig. 8. Representative XP-2p spectrum of complexes, the displayed spectra is of the Mn_5IP6. Each doublet line was fitted using a Gaussian–Lorentzian doublet function with 0.6 eV for doublet splitting.

$MnZn_4IP6$: 136.9 and 136.2 eV, respectively. Similar values were reported for $Zr[O_3POC_{10}H_{21}S]$ and $Mn[O_3POC_{30}H_{47}N_2]$ [35,36].

The XP-O1s photoelectric lines for all compounds showed asymmetric line-shapes that were fitted with three Gaussian–Lorentzian functions with binding energy values of (530.2 ± 0.3), (532.1 ± 0.3) and (534.2 ± 0.3) eV assigned to P–O–C, P–O–Zn(II) or P–O–Mn(II) and P═O, and possibly P–O–P or shake-up satellite, respectively (Fig. 9) [34,37]. Water molecules coordinated to transition metal complexes have a typical value for O1s binding energy of 532 eV, and therefore, could not be distinguished from oxygen in the P–O-Metal bond [15,16]. The P–O–P bonding could be formed by dehydration of two phytic acids in a similar way to phosphates, however, no other photoelectric line or spectroscopic result supports this assignment, therefore, we believe the peak is due to a shake-up satellite.

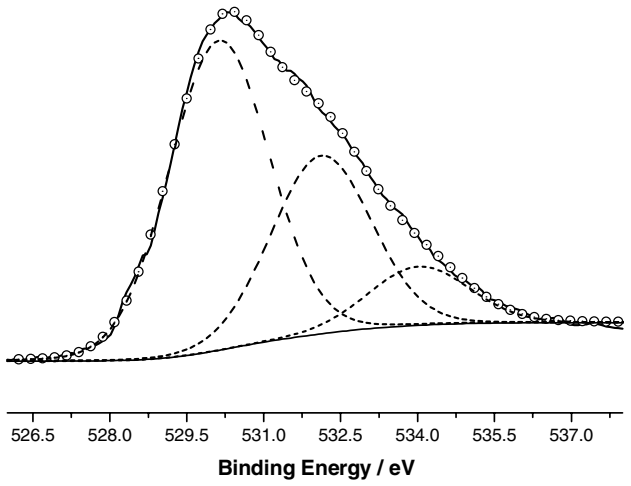

Fig. 9. Representative XP-O1s spectrum for the Zn(II) and manganese phytates. The spectrum shown is of the Mn_5IP6 complex.

4. Discussion

Elemental analysis and XPS both point to the same molecular formula where the metal-to-phytate ratio is ca. of 5:1 in agreement with previously reported data [12,13]. The phytate molecule in the metal phytates discussed in this article is in the 5 axial/1 equatorial conformation according to the ^{31}P results. This is in agreement with the reported results in solution which shows 5 axial/1 equatorial conformation to be the more stable one in basic pH. The vibrational spectroscopic data and the XP-P2p results indicate a bidentate coordination mode; however, XP-P2p and XP-O1s results point to two different phosphate groups in the complexes probably resulting from the presence of P–O–Na groups. ^{31}P MAS NMR analysis of the line-widths suggest that Na^+ anions are more loosely bound to phosphate in transition metal phytates than in dodecasodium phytate, occupying probably the third coordination sphere of P(V).

Based on the XP-Zn2p results only one Zn coordination environment is observed in Zn_5IP6 and $MnZn_4IP6$, however Mn has two different Zn environments in Mn_5IP6. The presence of P–O–P groups is ruled out by NMR data, so the higher binding energy mode is probably due to a shake-up satellite of the phosphate group. The simulation of EPR spectra for the $MnZn_4IP6$ results in two sets of Mn(II)-phytate environments, the first one with a larger zero field interaction and magnetic dipolar broadening and the second one with a smaller zero field and dipolar broadening. Using van Vleck's equation [38] for second moments to estimate line broadening, we can estimate an average distance between Mn(II) to be 8 Å for the first environment and 13 Å for the second environment. It was inferred that the first environment has two Mn(II) in the same phytate ring while the second environment has only one Mn(II) per ring.

Based on these results and the low solubility of these compounds in polar solvents like water, acetone, dimethylformamide and dimethylsulfoxide, we propose a supramacromolecular structure for the compounds as represented in Fig. 10. The solubility for all compounds in water at 353 K is ca. of 83 μM.

Monomeric species of manganese or Zn(II) phytate have been studied in aqueous solution by potentiometry, since these species are soluble. The presence of bridging Mn as shown in Fig. 10 would result in a large increase in the molecular weight and a decrease of total net charge resulting in a loss of solubility. Also, the presence of bridging and non-bridging Mn(II) species would explain the presence of two components in the XP-Mn2p

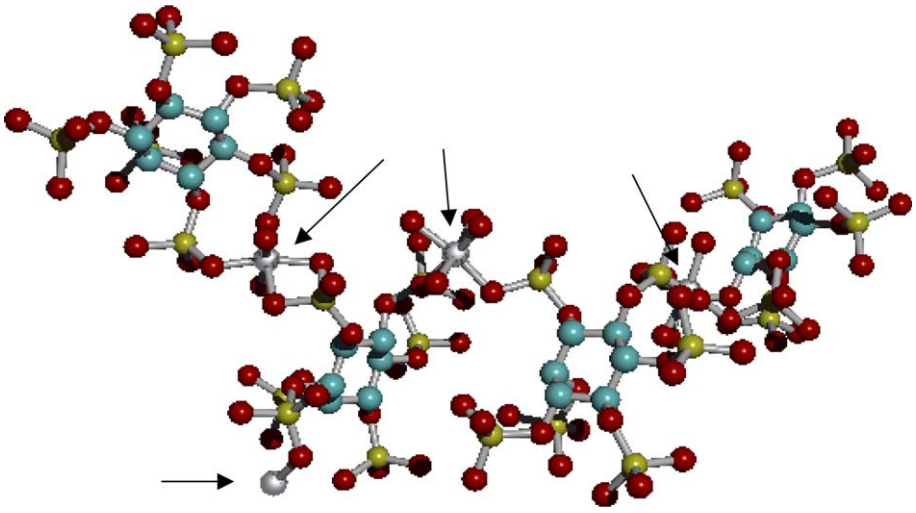

Fig. 10. The scheme shows the possible coordination chemical environments for Mn(II) ions in the three-dimensional network for metal phytates using Mn_5IP6 as an example. The manganese atoms are grey balls. In the $MnZn_4IP6$ the unit shown could have Mn and Zn in different ratios and the Mn–Mn distance could be 6.5–11 Å. Hydrogen atoms are omitted.

spectrum. The same is not observed in Zn(II) compounds probably because the 2p binding energy of this metal is not as sensitive as Mn2p. The proposed structure is in agreement with the EPR results and the broad line would be due to vicinal Mn(II).

5. Conclusion

The manganese complex in wheat seeds from Brazil and Denmark contain a heterometallic diamagnetic transition metal manganese phytate complex, probably containing Zn(II). A model compound of Zn(II) and manganese phytate was synthesized and spectroscopically characterized for the first time as $Na_4MnZn(II)_4(C_6H_6O_{24}P_6)\cdot(NO_3)_2\cdot 8H_2O$. In addition, other model Zn(II) phytate and manganese phytate complexes have been synthesized as $Na_3Mn_5(C_6H_6O_{24}P_6)OH\cdot 9H_2O$ and $Na_3Zn(II)_5(C_6H_6O_{24}P_6)OH\cdot 9H_2O$. In the manganese compounds, it was possible to identify two different chemical environments for the Mn(II) species, the first one coordinated to more than one phosphate and the other to only one phosphate group of phytate, IP6. These different chemical environments can lead to different chemical reactivity of the Mn in Mn_5IP6 and metal bioavailability. Further studies on the redox reactivity and structure of Mn_5IP6 complexes could also show their role as anti-oxidant natural compounds related to the presence of two different redox centers.

Acknowledgments

Dr. Marcella P. Felicissimo and Dr. Marciela Scarpellini are thankful to FAPESP for their PhD and post-doctoral fellowships. Professor Ubirajara P Rodrigues-Filho acknowledges the support of the Pró-Reitoria de Pós-Graduação of University of São Paulo and KVL for the fellowship for the short-term stay in Denmark at the beginning of this project. U.P.R.F. thanks to Professor Douglas W. Franco, University of São Paulo, for encouraging us to start this work.

Appendix A. Supplementary data

Supplementary data associated with this article can be found, in the online version, at doi:10.1016/j.jinorgbio.2005.06.014.

References

[1] D.C. Billington, The Inositol-phosphates, VCH, New York, 1993.
[2] M. Cheryan, Crit. Rev. Food Sci. Nutr. 13 (1980) 297–335.
[3] E. Miyazawa, A. Iwabuchi, T. Yoshida, Nutr. Res. 16 (1996) 603–613.
[4] D. Oberleas, J. Inorg. Biochem. 62 (1996) 231–241.
[5] E. Graf, J.W. Eaton, Free Rad. Biol. Med. 8 (1990) 61–69.
[6] F. Crea, P. Crea, A. De Robertis, S. Sammartano, Chem. Spec. Bioaval. 16 (2004) 16, 53–59.
[7] B.F. Harland, S. Smikle-Willians, D. Oberleas, J. Food Composit. Anal. 17 (2004) 227–233.
[8] T. Obata, Brain Res. 978 (2003) 241–244.
[9] V. Raboy, Phytochemistry 64 (2003) 1033–1043.
[10] F. Grases, L. Garcia-Ferragut, A. Costa-Bauzá, Urol. Res. 24 (1996) 305–311.
[11] I. Ockenden, J.A. Dorsch, M. Reid, L. Lin, L.K. Grant, V. Raboy, J.N.A. Lott, Plant Sci. 167 (2004) 1131–1142.
[12] A. Bebot-Brigaud, C. Dange, N. Fauconnier, C. Gerard, J. Inorg. Biochem. 75 (1999) 71–78.
[13] A.G. Pierce Jr, Inorg. Chim. Acta 106 (1985) L9–L12.
[14] S.J. Opella, M.H. Frey, J. Am. Chem. Soc. 101 (1979) 5854–5856.

[15] J.F. Mouder, W.F. Sticke, P.E. Sobol, K.D. Bombem, Handbook of X-Ray Photoelectron Spectroscopy, Perkin-Elmer, Eden Prairie, MN, 1992.
[16] NIST X-ray Photoelectron Spectroscopy Database, Version 3.4 (web version), Standard Refeference Data Program Database 20, National Institute of Standards and Technology, Gaithersburg, 2003. Available from: <http://srdata.nist.gov/xps/>.
[17] J.H. Scofield, J. Electron. Spectrosc. Rel. Phenom. 8 (1976) 129–137.
[18] G. Leclercq, J.-J. Pireaux, J. Electron. Spectrosc. Rel. Phenom. 71 (1995) 141–164.
[19] J.J. Windle, J.J. Evans, Cereal Chem. 48 (1971) 351.
[20] J.J. Chinoy, Y.D. Singh, M.M. Laloraya, Biochem. Physiol. Pflanzen 165 (1974) 536–540.
[21] H. Yoshioka, S. Tsuyumu, Agric. Biol. Chem. 52 (1988) 2977–2979.
[22] H. Yoshioka, S. Tsuyumu, K. Takayanagi, Agric. Biol. Chem. 54 (1990) 203–204.
[23] H. Yoshioka, K. Rin, S. Tsuyumu, Agric. Biol. Chem. 54 (1990) 3105–3110.
[24] B.A. Goodman, B. Williamson, J.A. Chudek, New Phytol. 122 (1992) 529–535.
[25] E.C. Pascual, B.A. Goodman, C. Yeretzian, J. Agric. Food Chem. 50 (2002) 6114–6122.
[26] R.G. Saifutdinov, L.I. Larina, T.I. Vakul'skaya, M.G. Voronkov, Electron Paramagnetic Resonance in Biochemistry and Medicine, Kluwer Academic/Plenum Publishers, New York, 2001.
[27] K.M. Schaich, C.A. Rebello, Cereal Chem. 76 (1999) 748–755.
[28] N. Abidi, B. Deroide, J.V. Zanchetta, M. Haddad, Phys. Chem. Glasses 40 (1999) 193–198.
[29] H.W. de Wijn, R.F. van Balderen, J. Chem. Phys. 46 (1967) 1381–1387.
[30] K. Nakamoto, Infrared and Raman Spectra of Inorganic Coordination Compounds, fourth ed., Wiley, New York, 1982.
[31] L.R. Isbrandt, R.P. Oertel, J. Am. Chem. Soc. 102 (1980) 3144–3148.
[32] R. Brow, C. Phifer, G. Turner, J. Kirkpatrick, J. Am. Ceram. Soc. 74 (1991) 1287–1290.
[33] C. De Stefano, D. Milea, A. Pettignano, S. Sammartano, Anal. Bioanal. Chem. 376 (2003) 1030–1043.
[34] R.K Brow, J. Non-crystal. Solids 194 (1996) 267–273.
[35] M.A. Petruska, D.R. Talham, Chem. Mater. 10 (1998) 3672–3682.
[36] X. Wang, M. Lieberman, Langmuir 19 (2003) 7346–7353.
[37] C.T. Seip, D.R. Talham, Mater. Res. Bull. 34 (1999) 437–445.
[38] J.H. van Vleck, Phys. Rev. 74 (1948) 1168–1183.